Nanoscale

COMMUNICATION

View Article Online
View Journal | View Issue

In situ growth of Au nanocrystals on graphene oxide sheets†

Cite this: *Nanoscale*, 2014, **6**, 1281

Received 4th September 2013
Accepted 15th November 2013

DOI: 10.1039/c3nr04714h

www.rsc.org/nanoscale

Yong Qin,[ab] Juan Li,[a] Yong Kong,*[a] Xiazhang Li,[a] Yongxin Tao,[a] Shan Li[a] and Yuan Wang[a]

Au nanocrystals (AuNCs) with a size of 10–20 nm decorated on graphene oxide (GO) were fabricated successfully through a hydrothermal reduction and crystallization route without any extra reductants and capping agents. The hydrophobic areas of GO benefit the formation of nanocrystals (NCs) with {111} facets totally exposed; however, the hydrophilic areas are detrimental to the crystallization. The morphology of AuNCs could be tailored by the degree of oxidation on the GO surface. The shape-controllable and reducing properties of GO are in favor of "clean" synthesis of noble metal NCs decorated on graphene.

Introduction

The construction of functional noble metal nanocrystals (NCs) such as Au, Pt and Pd NCs has attracted much interest because their unique optical, magnetic, and catalytic properties are tuneable by controlling the size, shape, chemical composition, and surface or interfacial structure. Noble metal NCs have many potential applications such as in catalysis, biodiagnostics, plasmonics, and surface-enhanced Raman scattering (SERS) spectroscopy.[1] The size- and shape-dependent properties of NCs have stimulated research into noble metal NCs of various shapes, such as wires,[2] rods,[3] prisms,[4] plates,[5] polyhedra,[6] and branched nanostructures.[7]

As a single layer of carbon atoms, graphene is fully comprised of a surface with high conductivity and specific surface area,[8] and so it is not surprising that the utilization of graphene sheets as a support for NCs could present promising features in new hybrids, such as enhanced electron transport rate and structural stability, due to the spatial confinement and synergetic electronic interactions between metallic and graphene components.[9] It has been found that metal NCs growing on graphene exhibit specific electronic[10] and catalytic[11] properties. Recent progress in synthetic technologies has made it possible to prepare metal NCs on a prefunctionalized graphene sheet through a chemical reduction route.[12] However, these approaches suffer from poor control over the size and structure of NCs due to difficulties in controlling the nucleation and growth process. Furthermore, these chemical routes usually require reductants or capping agents, such as surfactants[13] and polymers,[14] which would introduce "impurity" into the resultant hybrids. Therefore, developing an effective and facile approach to prepare homogeneous metal NCs on graphene sheets remains highly desirable.

In this communication, a clean method for *in situ* growth of Au nanocrystals (AuNCs) on graphene oxide (GO) was presented. In contrast to traditional strategies using reductants and capping agents, this method is free of reductants and capping agents because GO amazingly plays the role of reductants and capping agents simultaneously in the synthetic procedure. The morphology of AuNCs can even be tailored by the degree of oxidation on the surface of GO. The as-prepared AuNCs decorated on the GO composite display good SERS activity.

Experimental

GO was prepared from natural graphite flakes by using an improved Hummers' method.[15] Typically, graphite flakes (1.0 g) and $KMnO_4$ (6.0 g) were added into a mixture of 120 mL concentrated H_2SO_4 and 13.3 mL H_3PO_4, producing a slight exotherm at 35 °C. The mixture was then heated to 50 °C and stirred for 12 h. The reaction was cooled to room temperature and poured into ice water (150 mL) with 30% H_2O_2 (10 mL). The mixture was sifted through a polyester fibre. The filtrate was centrifuged (4000 rpm for 4 h), and the supernatant was decanted. The remaining solid material was then washed in succession with 200 mL of water, 200 mL of 30% HCl, and 200 mL of ethanol. The eventual solution was centrifuged (4000 rpm for 4 h) and the supernatant was decanted. The

[a]*College of Petrochemical Engineering, Changzhou University, Changzhou 213164, China. E-mail: yzkongyong@126.com; Fax: +86-519-86330167; Tel: +86-519-86330256*

[b]*College of Material Science and Engineering, Georgia Institute of Technology, Atlanta, 30332, USA*

† Electronic supplementary information (ESI) available: Fig. S1–S4. See DOI: 10.1039/c3nr04714h

solid was vacuum-dried overnight at room temperature, obtaining 1.8 g GO.

The AuNC–GO composites were synthesized in two steps. In the first step, 10 mL of 1 mg mL^{-1} GO and 0.1 mL of 0.4 mg mL^{-1} $HAuCl_4$ aqueous solution were mixed together at 80 °C with vigorous stirring for 1 hour to form a seed solution. The seed solution was cooled slowly to room temperature, and placed overnight. Subsequently the seed solution was mixed with 2 mL of 0.4 mg mL^{-1} $HAuCl_4$ and poured into a 50 mL polytetrafluoroethylene autoclave and hydrothermally treated overnight at 60 °C to form AuNCs. To decrease the oxygen content of GO, GO was pretreated hydrothermally at different temperatures before the preparation of AuNCs. The synthesis of Pt and Pd NCs supported on GO was performed by replacing the corresponding precursor with H_2PtCl_6 and H_2PdCl_4.

The morphologies were examined with a JEM-2000 transmission electron microscope (TEM) with an acceleration voltage of 200 kV. All TEM samples were prepared by depositing a drop of diluted solution on a copper grid coated with carbon films. X-ray photoelectron spectroscopy (XPS) analysis was performed on a PHI Quantum 2000 Scanning ESCA Microprobe with a monochromatised microfocused Al X-ray source. The X-ray diffraction (XRD) patterns were measured with an X'Pert Philips Materials Research Diffractometer using Cu/K_α radiation.

Results and discussion

Fig. 1a and b show low-resolution transmission electron microscopy (TEM) images of the resulting AuNC–GO composites, in which the layered GO serves as a support uniformly decorated with polyhedral AuNCs. These AuNCs consist of about 80% of pentagonal pyramid and 20% of tetrahedron with a size of 10–20 nm. Despite their irregular shape, they have excellent crystallinity and clear facet boundaries. The HRTEM image in Fig. 1c shows that the interplanar spacing of the AuNC lattice is 0.24 nm, which agrees well with the {111} lattice spacing of face-centered cubic (fcc) Au (0.24 nm).[16] As highlighted by FFT of the HRTEM image (Fig. 1c, inset), AuNCs only orient along the {111} direction. This result is also confirmed by the XRD pattern (Fig. 1d). The peak centred at $2\theta = 38.2$ corresponds to {111} facets of AuNCs, which is the only diffraction of Au in the XRD pattern.[17] Moreover, the XRD pattern also shows two characteristic peaks corresponding to GO ($2\theta = 10.2$) and graphene ($2\theta = 23.0$) respectively.[18] It is indicated that GO is partially reduced to graphene during the hydrothermal procedure, which is also confirmed by XPS. Comparison with the binding energy of C_{1s} on the GO surface (Fig. 2) clearly shows that after the reaction the oxygen content of GO is obviously decreased. These results suggest that the oxygenated functional groups on the GO surface play the role of reductants in the formation of AuNCs, which coincides with the results found by Chen *et al.*[19] The Au $4f_{7/2}$ and Au $4f_{5/2}$ peaks at *ca.* 83.8 and 87.6 eV are consistent with the Au^0 state (Fig. S1†),[20] further testifying the presence of metallic Au. Comparison with the UV-vis adsorption spectra of GO, AuNC–GO, mixture of GO and AuNCs shows that AuNCs have no obvious absorption peak but a platform in the visible light region, as shown in Fig. S2,† which suggests that AuNCs do not mechanically mix with GO, but are decorated on GO sheets. GO coated on the AuNC surface absorbs partial visible light, thus decreasing the absorption of AuNCs.

To better understand the AuNC growth process, we fabricated two other kinds of AuNCs decorated on GO with a lower degree of oxidation. The decrease of oxygen content is realized by hydrothermal reduction technology. As confirmed by XPS, after a hydrothermal pretreatment at 80 °C and 90 °C, the oxygen content of GO decreased from 20% to about 10% and 5% respectively. TEM images of AuNCs decorated on hydrothermal pre-treated GO with different degrees of oxidation are shown in Fig. 3. We can see that the amount of AuNCs on the lower degree oxidation of GO is much less than that on higher ones, which can also be confirmed by thermogravimetry analysis (TGA) (Fig. S3†). The main reason is that GO lost many reduction sites after the hydrothermal pre-treatment, which agrees well with the result of XPS that oxygenated functional groups on the GO surface play the role of reductants in the formation of AuNCs.

Fig. 3 also shows that AuNCs on GO with 10% oxygen content consist of about 90% of pentagonal pyramid, but AuNCs on GO with 5% oxygen are nearly total pentagonal pyramid. Compared to GO containing 20% oxygen (Fig. 1), AuNCs on GO with lower degree of oxidation have more uniform size and more regular

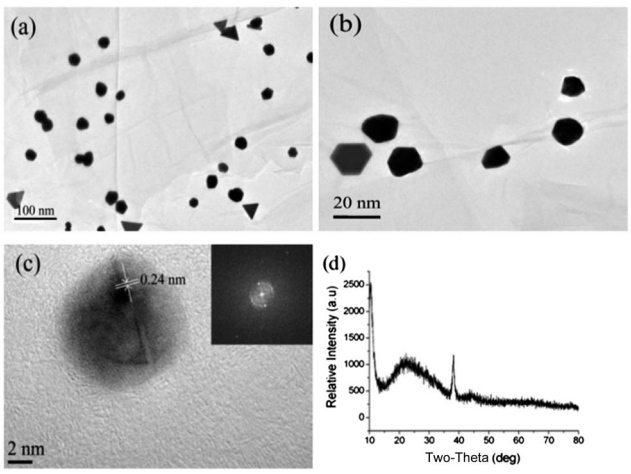

Fig. 1 Low (a and b) and high (c) resolution TEM images, and XRD pattern (d) of AuNCs decorated on GO with 20% oxygen. The inset in (c) is the fast Fourier transform (FFT) of the high resolution TEM (HRTEM) image.

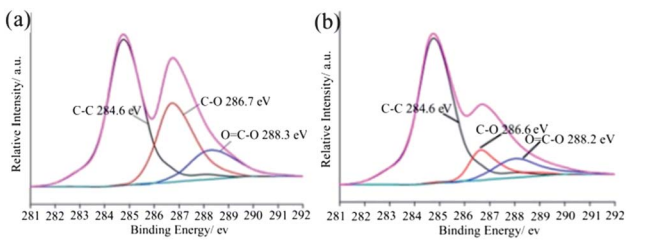

Fig. 2 XPS of C_{1s} on GO (a) and AuNC–GO (b) with 20% oxygen.

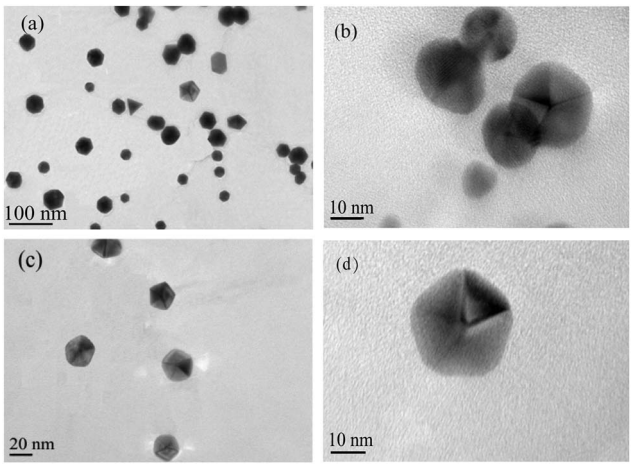

Fig. 3 TEM images of AuNCs decorated on GO with 10% (a and b) and 5% (c and d) oxygen.

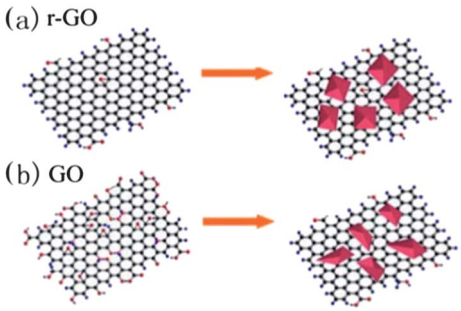

Fig. 4 Schematic AuNC growth on graphene with low (a) and high (b) degree of oxidation.

morphology, especially AuNCs on the surface of GO with 5% oxygen content, they are nearly perfect pentagonal pyramids with an equal side length of 13 nm (Fig. 3d), which indicates that the morphology of AuNCs growing on graphene depends on the degree of oxidation underlying graphene. The lower degree of oxidation of GO, the more regular morphology AuNCs (as illustrated in Fig. 4). We consider that GO with fewer functional groups and defects exhibits weaker chemical interactions with Au on the surface. The higher density of oxygen functional groups, including carboxylic, hydroxyl, and epoxy groups, on the GO surface interacts more strongly with Au atoms, providing pinning forces to the small particles to hinder diffusion and recrystallization. Increasing the hydrothermal crystallization temperature eventually leads to diffusion and recrystallization of surface species into larger crystals on GO, but AuNCs are more irregular (Fig. S4†). In fact, this shape-controlled function of GO is not limited to Au species. Dai *et al.*[21] had also found that the morphology of metal oxide or hydroxide NCs such as Fe_2O_3 and $Ni(OH)_2$ could also be tailored by the degree of oxidation of GO. Unlike pentagonal AuNCs, metal oxide or hydroxide NCs formed on GO was hexagonal.

Although the AuNC morphology depends on the degree of oxidation of GO, AuNCs always maintain the structure with {111} facets totally exposed. Why are Au atoms prone to pile up on GO in this way? According to the result of the density functional theory (DFT) calculation,[22] metals decorated on graphene are divided into two groups. Graphene chemisorbs Co, Ni, and Pd, leading to binding energies $E \sim 0.1$ eV per carbon atom. In contrast, graphene absorbs Al, Cu, Ag, Au, and Pt, leading to weaker binding energies $E \sim 0.04$ eV per carbon atom. Consequently, Co, Ni, and Pd can bind strongly on the surface of graphene, but Al, Ag, Au and Pt can only be absorbed weakly. It is likely that the interface between hydrophobic areas of GO and hydrophilic Au atoms exists relatively high interfacial energy. To decrease the interfacial energy, Au atoms adopt {111} facet orientation because the {111} planes of fcc crystals have the lowest surface energy. It resembles how water droplets form spherical drops on lotus leaves to lower the interfacial energy. Recently, Zettl *et al.*[23] observed an analogous phenomenon directly that Pt atoms oriented along {111} on graphene by high-resolution TEM using graphene cell technology. We also try to fabricate other noble metals such as Pt and Pd NCs decorated on the graphene composite. The results are shown in Fig. 5. Pt NCs have the space of lattice fringe $d = 0.22$ nm, which corresponds to the space of Pt {111} facets. In the XRD pattern, the diffraction peak at $2\theta = 39.6$ is assigned to the characteristic {111} crystalline plane of Pt (JPCDS: 87-0647) (Fig. 5a), which indicates that Pt easily forms flower-like NCs with {111} facets exposed like AuNCs. However, Pd nanoparticles showed different crystalline forms with Au and Pd. As indicated by TEM images and the XRD pattern (Fig. 5b), it mainly forms amorphous nanoparticles (Fig. 5b), which agrees well with the result of DFT calculation.

It is well known that a great many high quality NCs can now be prepared on the basis of solution chemistry methods.[24] However, various surfactants and polymers are usually required as capping agents to tune the growth processes. The surfaces of these materials are not clean because they are inevitably covered with long chain organic ligands, which will adversely discount the contributions of size and shape in practical applications, especially in catalytic fields. However, in this method, GO plays the role of capping agents and reductants, so it is very clean because it is free of any additives. This method brings further directions to prepare other "clean" noble metal NCs, such as Ag on graphene.

Noble metal NCs exhibit an optical phenomenon known as SERS in which the Raman scattering cross-sections are dramatically enhanced for the molecules adsorbed thereon.[25]

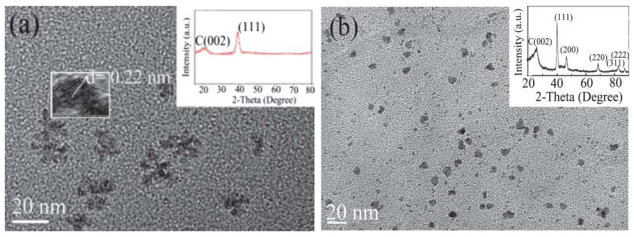

Fig. 5 TEM images and XRD (inset) of flower-like Pt NCs (a) and Pd nanoparticles (b) decorated on GO with 20% oxygen.

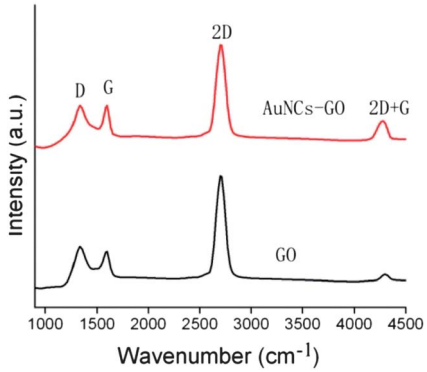

Fig. 6 The Raman spectra of GO and AuNC–GO with 5% oxygen.

Research has shown that the Raman signals of GO or graphene can be significantly enhanced in the presence of metal NCs, with enhancement factors ranging from a few times up to tens of times.[26] The SERS spectra of GO and AuNCs decorated on GO with low degree of oxidation are shown in Fig. 6.

Four characteristic bands are observed at 1350, 1600, 2710 and 4300 cm^{-1} corresponding to the D band, G band, 2D band and combination band respectively. The D band is a breathing mode of *k*-point phonons of the A_{1g} symmetry, while the G band is usually assigned to the E_{2g} phonon of C sp^2 atoms. There are almost no significant differences in the intensity ratio of I_D/I_G between AuNC–GO nanocomposites and GO, suggesting that the attachment of AuNCs does not change the size of in plane sp^2 domains. It has been reported that variations of I_{2D}/I_G ratios and shifts of G and 2D bands are related to doping of graphene.[27,28] Fig. 6 shows that the changes of I_{2D}/I_G ratios from 2.5 to 1.4 after AuNCs are loaded, which also indicates that AuNCs are bound on GO, but not mechanically mixed with GO. Fig. 6 also shows that Raman signals of graphene have been significantly enhanced after decorating AuNCs. Both D and G bands of the AuNC–GO composite are significantly higher than those of the pure GO. The obtained SERS enhancement factors are about 4, which are consistent with the previously reported SERS studies on GO.[29] These studies on the enhanced optical properties of AuNC–GO composites could be utilized to develop various applications such as chemical, biological sensing and imaging.

Conclusions

In summary, we found that *in situ* growth of Au atoms on GO without any extra additives could produce 10–20 nm pentagonal pyramid AuNCs with {111} facets exposed. The morphology of AuNCs on GO can be tailored by the degree of oxidation of graphene. The hydrophobic areas of GO play the role of capping agents, and control the formation of NCs with {111} facets totally exposed. The hydrophilic areas of GO play the role of reductants, and interfere with the crystallization. The whole process is very "clean" because it is free of capping agents and reductants. The as-prepared AuNC decorated GO composite has good performance to SERS. This facile method is also suitable to fabricate other clean noble metal NCs, such as Ag, Pt decorated on GO.

Acknowledgements

This work was supported by NSFC (no. 21275023, no. 51002016), the Project of Young Teacher Overseas Training of Jiangsu, and the Priority Academic Program Development of Jiangsu Higher Education Institutions (PAPD).

Notes and references

1 (*a*) C. Zhu, J. Zeng, J. Tao, C. M. Johnson, I. Schmidt-Krey, L. Blubaugh, Y. M. Zhu, Z. Z. Gu and Y. N. Xia, *J. Am. Chem. Soc.*, 2012, **134**, 15822; (*b*) C. C. Li, K. L. Shufold, M. H. Chen, E. J. Lee and S. Q. Cho, *ACS Nano*, 2008, **2**, 1760; (*c*) C. H. Kuo, Y. C. Yang, S. Gwo and M. H. Huang, *J. Am. Chem. Soc.*, 2011, **133**, 1052; (*d*) W. C. Wang, L. M. Lyu and M. H. Huang, *Chem. Mater.*, 2011, **23**, 2677; (*e*) M. Mulvihill, A. Tao, K. Benjauthrit, J. Arnold and P. Yang, *Angew. Chem., Int. Ed.*, 2008, **47**, 6456.
2 G. Schider, J. R. Kreen, W. Gotschy, B. Lamprecht, H. Ditlbacher, A. Leitner and F. R. Aussenegg, *J. Appl. Phys.*, 2001, **90**, 3825.
3 A. S. Stender, G. F. Wang, W. Sun and N. Fang, *ACS Nano*, 2010, **4**, 7667.
4 F. Lu, Y. Zhang, L. H. Zhang, Y. G. Zhang, J. X. Wang, R. R. Adzic, E. A. Stach and O. Gang, *J. Am. Chem. Soc.*, 2011, **133**, 1074.
5 B. B. Cao, B. Liu and J. H. Yang, *CrystEngComm*, 2013, **15**, 5735.
6 S. J. Lee, G. Park, D. Seo, D. Ka, S. Y. Kim, I. S. Chung and H. Song, *Chem.–Eur. J.*, 2011, **17**, 8466.
7 E. C. Hao, R. C. Bailey, G. C. Scchatz, J. T. Hupp and S. Y. Li, *Nano Lett.*, 2004, **4**, 327.
8 K. S. Novoselov, A. K. Geim, S. V. Morozov, D. Jiang, Y. Zhang, S. V. Dubonos, I. V. Grigorieva and A. A. Firsov, *Science*, 2004, **306**, 666.
9 Y. Liang, Y. Li, H. Wang, J. Zhou, J. Wang, T. Regier and H. Dai, *Nat. Mater.*, 2011, **10**, 780.
10 H. Wang, L. Cui, Y. Yang, H. Casalongue, J. Robinson, Y. Liang, Y. Cui and H. Dai, *J. Am. Chem. Soc.*, 2010, **132**, 13978.
11 S. J. Guo and S. H. Sun, *J. Am. Chem. Soc.*, 2012, **134**, 2492.
12 B. S. Yin, H. Y. Ma, S. Y. Wang and S. H. Chen, *J. Phys. Chem. B*, 2003, **107**, 8898.
13 L. Zhang, W. Niu and G. Xu, *Nano Today*, 2012, **7**, 586.
14 Z. Tang, S. Shen, J. Zhuang and X. Wang, *Angew. Chem.*, 2010, **122**, 4707.
15 D. C. Marcano, D. V. Kosynkin, J. M. Berlin, A. Sinitskii, Z. Sun, A. Slesarev, L. B. Alemany, W. Lu and J. M. Tour, *ACS Nano*, 2010, **8**, 4806.
16 Z. Wang, S. Zhao, S. Zhu, Y. Sun and M. Fang, *CrystEngComm*, 2011, **13**, 2262.
17 Y. Qin, R. Che, C. Liang, J. Zhang and Z. Wen, *J. Mater. Chem.*, 2011, **21**, 3960.
18 W. R. Collins, W. Lewandowski, E. Schmois, J. Walish and T. M. Swager, *Angew. Chem., Int. Ed.*, 2011, **50**, 8848.

19 X. Chen, G. Wu and J. Chen, *J. Am. Chem. Soc.*, 2011, **133**, 3693.
20 X. Yang, M. Xu, W. Qiu, X. Chen, M. Deng, J. Zhang, H. Iwai, E. Watanabe and H. Chen, *J. Mater. Chem.*, 2011, **21**, 8096.
21 H. Wang, J. T. Robinson, G. Diankov and H. Dai, *J. Am. Chem. Soc.*, 2010, **132**, 2070.
22 G. Giovannetti, P. A. Khomyakov, G. Brocks, V. M. Karpan, J. van Brink and P. J. Kelly, *Phys. Rev. Lett.*, 2008, **101**, 026803.
23 J. M. Yuk, J. Park, P. Ercius, K. Kim, D. J. Hellebusch, M. F. Crommie, J. Y. Lee, A. Zettl and A. P. Alivisatos, *Science*, 2012, **336**, 61.
24 S. Murphy, L. Huang and P. V. Kamat, *J. Phys. Chem. C*, 2013, **117**, 4740.
25 Y. H. Lee, L. Polavarapu, N. Gao, P. Yuan and Q. Xu, *Langmuir*, 2012, **28**, 321.
26 S. He, K. Liu, S. Su, J. Yan, X. Mao, D. Wang, Y. He, L. Li, S. Song and C. Fan, *Anal. Chem.*, 2012, **84**, 4622.
27 J. Lee, K. S. Novosolev and H. S. Shin, *ACS Nano*, 2011, **5**, 608.
28 L. Li, B. An, A. Lahiri, P. Wang and Y. Fang, *Carbon*, 2013, **65**, 359.
29 T. T. Baby and S. Ramaprabhu, *J. Mater. Chem.*, 2011, **21**, 9702.